Vector analysis of the current commutation in PM BLDC drives

Giuseppe Buja[1], Roberto Menis[2], and Ritesh Kumar Keshri[1]

Abstract - **Vector approach in either stationary or synchronous plane is commonly used for the analysis of the AC drives like induction and PM brushless AC drives whilst it has been hardly ever used for the PM brushless DC (BLDC) drives. A possible reason is that they require injection of square-wave currents into the motor phases, which are non-sinusoidal in nature. Recently, the PM BLDC drives have been analyzed by the help of the vector approach in the stationary plane. This paper applies such an approach to an in-depth analysis of the operation of the PM BLDC drives during the current commutations, illustrating the potentialities of the approach in giving a better insight into the current transients and the ensuing torque characteristics. At last, two voltage control strategies proposed to eliminate the torque ripple due to the current commutations are considered, showing that they can be readily understood by the vector approach.**

Index Terms— **PM BLDC drive; current commutation; stationary plane vector analysis.**

I. INTRODUCTION

PM BLDC drives are characterized by the capability of offering higher torque and power density compared to other AC drives of the same size. These features together with compact structure and cost effectiveness of the motor have made the PM BLDC drives widely accepted for motorizing many industrial equipment [1]-[3] and, nowadays, for propelling electric vehicle [4]-[6]. PM BLDC drives require injection of square-wave currents into the motor phases, synchronized with the flat portion of the trapezoidal back-emf to develop a constant torque and -at the same time- to maximize the torque-per-ampere ratio. As the flat portion of the back-emf covers 120° electrical angle, the voltage source inverter (VSI) supplying the motor uses its 120° working mode to inject square-wave currents into the motor phases. Commutation of the phase currents takes place with an electrical angle periodicity of 60° and should be instantaneous [7]. In practice, phase inductances and limited supply voltage yield a finite time for the commutations and the currents deviate from the required waveform. Any mismatch in the current waveform impairs the drive performance as it produces: i) a drop of the speed-torque characteristic at high speeds that limits the full utilization of the drive in all the speed range, and ii) the onset of torque ripples over almost all the speed range that give rise to an uneven motion of the attached mechanical load and an unduly solicitation on the rotor bearings [8]. Here, torque ripples designate the torque pulsations due to the current commutations. Other types of torque pulsations exist; they are due to the current oscillations originated by the PWM control of the VSI and to the cogging phenomena originated by the interaction between the permanent magnets of the rotor and the slots of the stator. Torque pulsations due to the current oscillations occur at high frequencies so that their impact on the load speed is very much attenuated by the filtering action of the motor-load inertia whilst torque pulsations due to the cogging phenomena are minimized with a suitable electromagnetic design of the motor [9].

Current transients in the PM BLDC drives during the commutations have been explained in [10] for the defined low and high speed zones. The profiles of the torque developed by the motor during the commutations have been derived in [11] as a function of the motor speed by correlating currents, speed and torque of the motor. All the significant literature on the matter has approached the analysis of the PM BLDC drives by means of the phase variables. Recently, this analysis has been executed by means of the vector representation of the drive variables in the stationary plane [12].

This paper applies the vector approach to an in-depth analysis of the operation of the PM BLDC drives during the current commutations. Organization of the paper is as follows: Section II reviews the vector representation of the PM BLDC drive variables in the stationary plane; Sections III and IV exploits the vector approach to illustrate the current transients during the commutations and the ensuing torque characteristics at low and high speeds, respectively; Section V shows the potentialities of the vector approach by using it to explain the rationale behind two voltage control strategies proposed in the literature to eliminate the torque ripple due to the current commutations [13], [14]; Section VI concludes the paper.

II. PM BLDC DRIVE

A. Operation

Circuital scheme of a conventional PM BLDC drive is shown in Fig. 1. The DC link of the drive is powered by the DC voltage source V_d and feeds the PM BLDC motor through the VSI.

Voltage equations for the motor phases are

G. Buja and R. K. Keshri are with Department of Industrial Engineering, University of Padova, Italy (email: giuseppe.buja@unipd.it, ritesh.keshri@studenti.unipd.it)

R. Menis is with Department of Engineering and Architecture, University of Trieste, Italy (email: menis@units.it).

$$\frac{di_j(\theta_e)}{d\theta_e} = -\frac{R}{\Omega_e L}i_j(\theta_e) + \frac{1}{\Omega_e L}\underbrace{\left[v_{jn}(\theta_e) - e_j(\theta_e)\right]}_{v_{jL}(\theta_e)} \quad j = a,b,c \quad (1)$$

where j is a generic motor phase, i_j, v_{jn}, v_{jL} and e_j are the current flowing into the motor phases, the voltages applied to the motor phases, the voltage drop across the phase inductances, and the back-emf of the motor phases, respectively, R and L are the resistance and the mutual-effect inclusive inductance of the motor phases, $\theta_e = \Omega_e t$ is the angular phase in electrical radians, $\Omega_e = n_p\Omega$ is the motor speed in electrical radians per second, n_p is the number of pole pairs, and Ω is the motor speed.
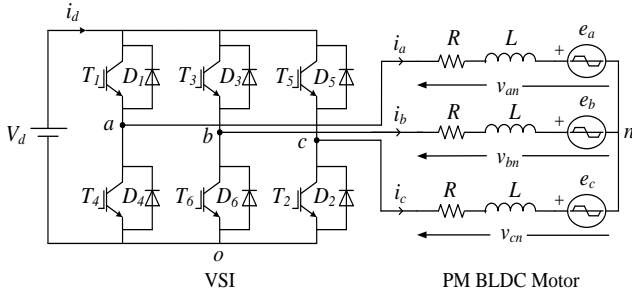

Fig. 1. Circuital scheme of a PM BLDC drive.

The phase voltages v_{jn} are related to the VSI output voltages v_{jo}, measured with respect to the negative rail of the DC link, by

$$v_{jo} = v_{jn} + v_{no} \quad (2)$$

and the phase currents are constrained by the Kirchhoff's current law

$$\sum_{j=a,b,c} i_j = 0 \quad (3)$$

The instantaneous electrical power p converted into mechanical form and the corresponding motor torque τ can be expressed as

$$p(\theta_e) = \sum_{j=a,b,c} e_j(\theta_e) i_j(\theta_e) \quad (4)$$

$$\tau(\theta_e) = \frac{p(\theta_e)}{\Omega} \quad (5)$$

Operation of a PM BLDC drive is expounded with the help of Fig. 2. Back-emfs are trapezoidal with the magnitude of the flat portions equal to $+E$ or $-E$ and their duration equal to $2\pi/3$ (electrical) radians. The value of E is given by

$$E = k\Omega \quad (6)$$

where k is the motor constant. The phase currents have a square waveform with pulses of magnitude $+I$ or $-I$ that are synchronized with the flat portions of the back-emf. For motor operation, the phase currents in Fig.2 have the same sign as the polarity of the back-emfs.

From Fig. 2, it emerges that the supply period of the motor can be divided into six supply intervals S_1, S_2, ..., and S_6 of the duration of $\pi/3$ radians. At the beginning of each supply interval, one phase starts to conduct (incoming phase) and another one finishes of conducting (outgoing phase). During the remaining part of the supply interval, only two-phases with back-emfs of opposite polarities conduct (conducting phases). To identify the supply interval and, from it, the conducting transistors of the VSI, the drive control uses the information delivered by three Hall sensors mounted on the stator and displaced of $2\pi/3$ electrical radians. The required voltage is applied to the conducting phases by stepping down the DC link voltage V_d through the choppering of the conducting transistors.
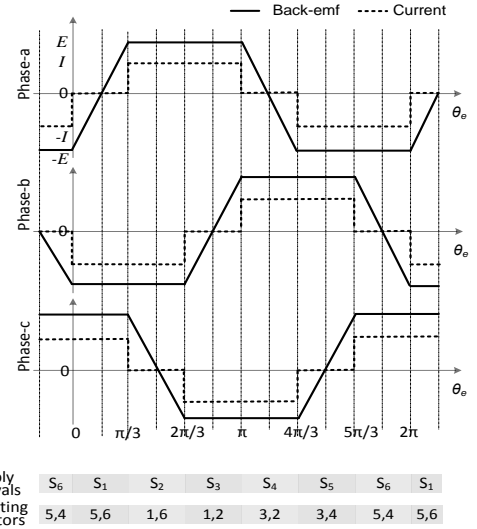

Fig. 2. Back-emfs, currents and supply intervals of a PM BLDC drive.

B. Control system

As Fig. 3 shows, regulation of the phase currents at the reference value I_{ref} can be accomplished by the closed-loop control of the DC link current i_d. In fact, this current remains equal to the current flowing into a motor phase when both the conducting transistors are ON; therefore, if properly sampled, the DC link current gives the feedback of the phase currents. The current error is processed by a PI regulator that delivers the required voltage v_c for the motor phases.

Application of v_c across the phases of the motor is commonly attained by chopping only one of the two conducting transistors to reduce the switching losses; a common strategy is to chop the transistor carrying either the incoming or the outgoing current. Hereafter, it is assumed that the control applies the required voltage without any delay.
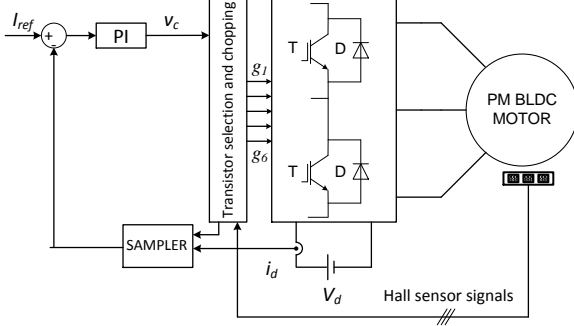
Fig. 3. Schematic of the control of a PM BLDC drive.

C. Stationary plane representation

Equations of the PM BLDC motor can be written in terms of the vectors $i = [i_\alpha \; i_\beta]^T$, $e = [e_\alpha \; e_\beta]^T$, and $v = [v_\alpha \; v_\beta]^T$ of the currents and the back-emfs of the motor phases, and the VSI output voltages in the stationary plane. The vectors, calculated with a magnitude-invariant transformation, are given by

$$i(\theta_e) = i_a(\theta_e) + j\frac{1}{\sqrt{3}}[i_b(\theta_e) - i_c(\theta_e)]$$

$$v(\theta_e) = \frac{2}{3}\left[v_{ao}(\theta_e) - \frac{v_{bo}(\theta_e)}{2} - \frac{v_{co}(\theta_e)}{2}\right] + j\frac{1}{\sqrt{3}}[v_{bo}(\theta_e) - v_{co}(\theta_e)] \quad (7)$$

$$e(\theta_e) = \frac{2}{3}\left[e_a(\theta_e) - \frac{e_b(\theta_e)}{2} - \frac{e_c(\theta_e)}{2}\right] + j\frac{1}{\sqrt{3}}[e_b(\theta_e) - e_c(\theta_e)]$$

By (7), the voltage equations in (1) become

$$\frac{d\,i(\theta_e)}{d\theta_e} = -\frac{R}{\Omega_e L}i(\theta_e) + \frac{1}{\Omega_e L}\underbrace{[v(\theta_e) - e(\theta_e)]}_{v_L(\theta_e)} \quad (8)$$

Calculation of the current and back-emf vectors for the waveforms in Fig. 2 shows that: i) the current vector i remains stationary within the supply intervals S_1, S_2, ..., and S_6, and coincides with the radii I_1, I_2, ..., and I_6, respectively, of an hexagon (current hexagon), ii) the back-emf vector e moves along the sides of an hexagon (back-emf hexagon) during the supply intervals, and coincides with the radii E_1, E_2, ..., and E_6 of the hexagon at the beginning of the supply intervals. Current and back-emf vectors are traced in Fig. 4 whilst their values as a fraction of I and E are reported in Tab. I.

As an example, in the supply interval S_1 the current vector jumps from I_6 ($-I$, $I/\sqrt{3}$) to I_1 (0, $-2I/\sqrt{3}$) at $\theta_e = 0$ and, after that, stays at I_1 within the whole S_1. Instead, the back-emf vector takes the value E_1 ($-2E/3$, $-2E/\sqrt{3}$) at $\theta_e = 0$ and moves towards E_2 ($2E/3$, $-2E/\sqrt{3}$) during S_1, reaching E_2 at $\theta_e = \pi/3$. For given values of I and E, the magnitude of the current vector remains the same and equal to $2I/\sqrt{3}$, whereas the magnitude of the back-emf vector undergoes a continuous change from the maximum value of $4E/3$ at the beginning of the supply interval to the minimum value of $2E/\sqrt{3}$ at the mid

of supply interval and then again to the maximum value of $4E/3$ at the end of the supply interval.

Power equation in (4) can be expressed in terms of the inner product of the vectors e and i as

$$p(\theta_e) = \frac{3}{2}e(\theta_e) \bullet i(\theta_e) = \frac{3}{2}[e_\alpha(\theta_e)i_\alpha(\theta_e) + e_\beta(\theta_e)i_\beta(\theta_e)] \quad (9)$$

For the ideal case of instantaneous commutation, during the interval $-0 \le \theta_e \le \pi/3$ the magnitude of the projection of e over i is constant and equal to $2E/\sqrt{3}$. Thus the motor torque in (5) turns out to be constant and equal to
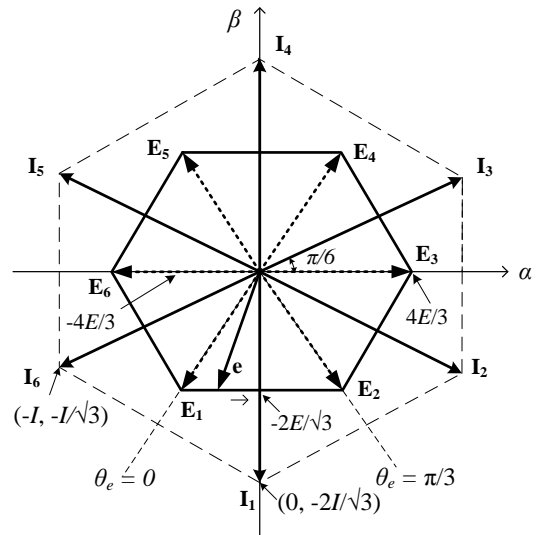
$$T = 2kI \quad (10)$$

Fig. 4. Current and back-emf vectors in the stationary plane.

TABLE I. CURRENT AND BACK-EMF VECTORS

Supply Interval	Current vectors as a fraction of I	Back-emf vectors as a fraction of E
S_1	$I_1 = -j\dfrac{2}{\sqrt{3}}$	$E_1 = -\dfrac{2}{3} - j\dfrac{2}{\sqrt{3}}$
S_2	$I_2 = 1 - j\dfrac{1}{\sqrt{3}}$	$E_2 = \dfrac{2}{3} - j\dfrac{2}{\sqrt{3}}$
S_3	$I_3 = 1 + j\dfrac{1}{\sqrt{3}}$	$E_3 = \dfrac{4}{3}$
S_4	$I_4 = j\dfrac{2}{\sqrt{3}}$	$E_4 = \dfrac{2}{3} + j\dfrac{2}{\sqrt{3}}$
S_5	$I_5 = -1 + j\dfrac{1}{\sqrt{3}}$	$E_5 = -\dfrac{2}{3} + j\dfrac{2}{\sqrt{3}}$
S_6	$I_6 = -1 - j\dfrac{1}{\sqrt{3}}$	$E_6 = -\dfrac{4}{3}$

III. CURRENT COMMUTATION

In practice, the incoming and outgoing currents take some time to get the required magnitude and the current commutation is not instantaneous. The analysis of the PM BLDC drive operation during the current commutations is

carried out by supposing that

i) the voltage drop across the phase resistances is negligible compared to the other voltage terms in (8), so that it can be disregarded,

ii) the commutation interval is small compared to the maximum allowed interval of $\pi/3$ [9] so that e remains equal to the back-emf vector taken at the beginning of the relevant supply interval.

Above assumptions reduce (8) to

$$\frac{d\,i(\theta_e)}{d\theta_e} = \frac{1}{\Omega_e L}\underbrace{[v(\theta_e) - E_1]}_{v_L(\theta_e)} \tag{11}$$

for the supply interval S_1. Eq. (11) shows that the change in the current vector is parallel to v_L.

Let us consider the current commutation taking place at the beginning of the supply interval S_1, which starts at $\theta_e = 0$ as in Fig. 2. The drive control system turns T_4 OFF and T_6 ON, and keeps T_5 ON. The commutating currents are i_b and i_a, with i_b that is ingoing and i_a that is outgoing, whilst i_c is the non-commutating current. Current i_a freewheels through D_1 until it extinguishes.

Generally, the commutation interval is divided into two subintervals, and the current transients depend on whether the motor runs in the low-speed zone, which occurs for $4E<V_d$, or in the high-speed zone, which occurs for $4E>V_d$ [10]. The current transients in the two speed zones and for $4E=V_d$ are shown in Fig. 5, where the duration of the commutation interval is denoted with θ_c, and the two commutation subintervals are marked with #1 and #2. Hereafter, quantities pertinent to the low-speed zone are identified with the subscript ℓ and those to the high-speed zone with the subscript h.

A. Current transients in subinterval #1

During subinterval #1, all the three motor phases conduct and the VSI exerts the maximum effort to the motor for the commutating currents to reach the required magnitudes, i.e. it is $v_{ao} = V_d$, $v_{bo} = 0$ and $v_{co} = V_d$. From (7), the vector of the VSI output voltages during subinterval #1 is

$$V_1 = \left(\frac{1}{3} - j\frac{1}{\sqrt{3}}\right)V_d \tag{12}$$

The vector has fixed magnitude and is aligned along $\mathbf{E_2}$. By (11) and (12), the vector of the voltage drops across the phase inductances is

$$V_{L,1} = V_1 - E_1 = \frac{1}{3}(V_d + 2E) - j\frac{1}{\sqrt{3}}(V_d - 2E) \tag{13}$$

The vector in (13) has a slope of

$$m_1 = -\sqrt{3}\left(\frac{V_d - 2E}{V_d + 2E}\right) \tag{14}$$

which is a function of E and, therefore, depends upon the motor speed Ω.

Integration of (11) with the initial condition $i(0) = I_6$ leads to the current vector i during subinterval #1

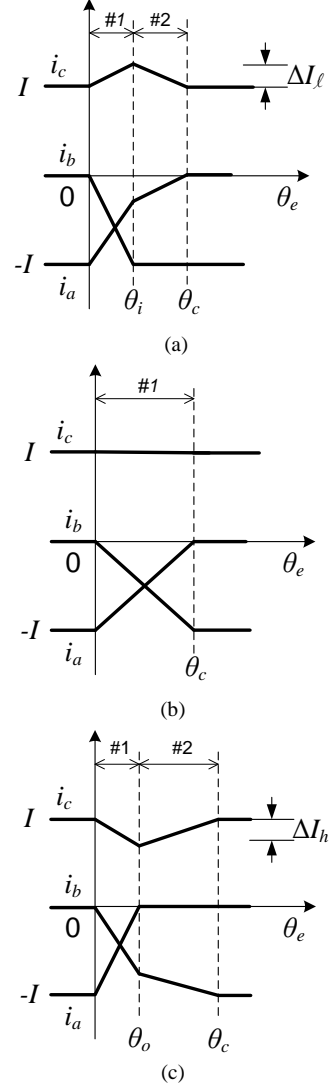Fig. 5. Current transients during commutation: a) in the low-speed zone ($4E<V_d$), b) for $4E=V_d$, and c) in the high-speed zone ($4E>V_d$)

$$i_1(\theta_e) = \frac{1}{\Omega_e L}\left[\frac{1}{3}(V_d + 2E) - j\frac{1}{\sqrt{3}}(V_d - 2E)\right]\theta_e + I_6 \tag{15}$$

From (14) and (15) it can be concluded that the current vector during subinterval #1 moves towards I_1 along a straight line with the slope in (14). So, as shown in Fig. 6, there are three possible trajectories of the tip of the current vector: i) in the low speed zone, i.e. for $4E<V_d$, m_1 is less than $-1/\sqrt{3}$ and the tip of i_1 moves along a line like x, which has an angular

slope in the range from $-\pi/6$ to $-\pi/3$, ii) for $4E=V_d$, m_1 becomes equal to $-1/\sqrt{3}$ and the tip of i_1 moves along the line joining I_6 and I_1, which has an angular slope of $-\pi/6$, and iii) in the high speed zone, i.e. for $4E>V_d$, m_1 becomes greater than $-1/\sqrt{3}$ and the tip of i_1 moves along a line like w, which has an angular slope in the range from 0 to $-\pi/6$.

Subinterval #1 ends in three possible modes: i) for $4E<V_d$, the incoming current i_b reaches the required magnitude $-I$ at the angle θ_i before that i_a the outgoing current vanishes [Fig. 5(a)]; ii) for $4E=V_d$, i_b reaches $-I$ at the same angle that i_a vanishes and the commutation completes at the end of the subinterval #1, [Fig. 5(b)], iii) for $4E>V_d$, i_a vanishes at the angle θ_o before that i_b reaches $-I$ [Fig. 5(c)]. In both the modes i) and iii), the commutation continues with a second subinterval where i_a vanishes and i_b gets the required magnitude; at the completion of this subinterval, denoted with #2, commutation is completed and the current vector becomes equal to I_1. Subinterval #2 lasts $\theta_{ci} = \theta_{c\ell} - \theta_i$ in mode i) and $\theta_{co} = \theta_{ch} - \theta_o$ in mode iii).
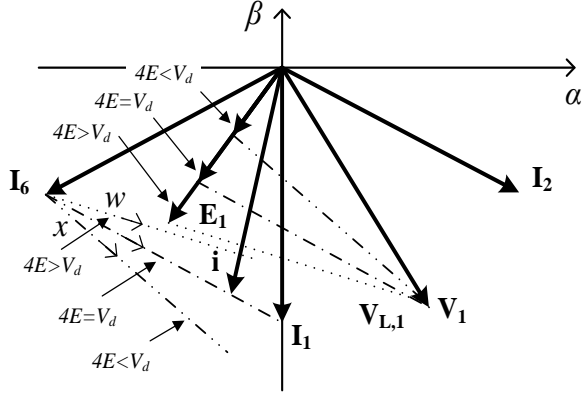

Fig. 6. Current vector trajectories during subinterval #1.

B. *Current transients in low-speed zone*

During subinterval #1 the tip of the current vector moves along a line like x, as explained in the previous Subsection. At the end of the subinterval #1, the current of phase b reaches the required magnitude $-I$, i.e. it is $i_{b\ell}(\theta_i) = -I$, while the current of phase a is still flowing.

During subinterval #2, the drive control system regulates i_b at $-I$ by applying the voltage $v_{bo} = V_d-E$ at the output b of the VSI, while the other two outputs of the VSI are kept at the same voltages as before, i.e. it is $v_{ao}=V_d$, and $v_{co} = V_d$, for i_a to vanish. The vectors of the VSI output voltages and the voltage drops across the phase inductances are expressed as

$$V_{2\ell} = \left(\frac{1}{3} - j\frac{1}{\sqrt{3}}\right)E \tag{16}$$

$$V_{L,2\ell} = \left(1 + j\frac{1}{\sqrt{3}}\right)E \tag{17}$$

Both the vectors have a magnitude that depends on the speed and a slope that is independent of the speed. In particular, the slope of the vector in (17) is

$$m_{2\ell} = \frac{1}{\sqrt{3}} \tag{18}$$

that, as shown in Fig. 7, is the same as the line s. Substitution of (17) into (11) and integration of (11) give the current vector in subinterval #2

$$i_{2\ell}(\theta_e - \theta_i) = \left(1 + j\frac{1}{\sqrt{3}}\right)\frac{E}{\Omega_e L}(\theta_e - \theta_i) + i_{1\ell}(\theta_i) \quad \theta_e > \theta_i \tag{19}$$

where $i_{1\ell}(\theta_i)$ is the current vector at the end of subinterval #1. The angle θ_i can be obtained by calculating the current vector at $\theta_e=\theta_i$ by means of the first equation in (7), which becomes

$$i_{1\ell}(\theta_i) = i_a(\theta_i) + j\frac{1}{\sqrt{3}}\left[-2I + i_a(\theta_i)\right] \tag{20}$$

Then, by equating the real and imaginary parts of (20) to (15), also calculated at $\theta_e=\theta_i$, the values of θ_i and $i_a(\theta_i)$ can be obtained. In particular, θ_i results in

$$\theta_i = \frac{3\Omega_e LI}{2(V_d - E)} \tag{21}$$

Finally, substitution of (21) into (15) yields $i_{1\ell}(\theta_i)$.

The trajectory of the tip of the current vector in subinterval #2, i.e. of $i_{2\ell}(\theta_e - \theta_i)$, is a straight line having the slope in (18). Since the current vector coincides with I_1 at the end of subinterval #2, and the slope of the vector $I_{21}=I_2 - I_1$ is the same as (18), the trajectory is represented by the line s of Fig. 7 that passes through the tips of the vectors I_1 and I_2. Thus, it can be stated that subinterval #1 ends when the line x intersects the line s.

Subinterval #2 finishes when the current vector reaches I_1. This occurs when the current of the phase a vanishes. Being i_a equal to the real part of the current vector, the duration of subinterval #2 can be obtained by equating to zero the real part of (19) calculated at $\theta_e=\theta_{c\ell}$. It is

$$\theta_{ci} \equiv \theta_{c\ell} - \theta_i = \frac{\Omega_e LI}{2E}\left(\frac{V_d - 4E}{V_d - E}\right) \tag{22}$$

and, from (21) and (22), the duration of the commutation interval is

$$\theta_{c\ell} = \frac{\Omega_e LI}{2E} \equiv \frac{n_p LI}{2k} \tag{23}$$
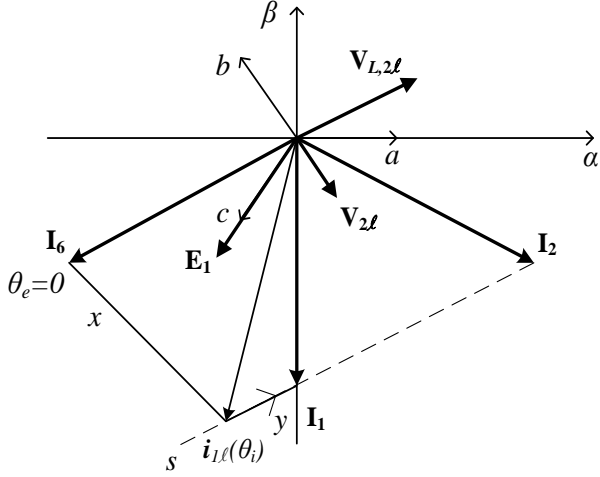
Fig. 7. Phase vectors during subinterval #2 in low-speed zone.

It is worth to note that the commutation interval does not depend on the motor speed and, furthermore, it coincides with the commutation interval as obtained for $4E=V_d$.

The transients of the phase currents in the low-speed zone drawn in Fig. 5 (a) can be readily found by projecting the current vector on the axes a, b, and c of Fig. 7.

C. Current transients in high-speed zone

During subinterval #1 the tip of the current vector moves along a line like w, as explained in Subsection A). At the end of the subinterval #1, the current of phase a vanishes, i.e. it is $i_{ah}(\theta_o)=0$, while the current of phase b is still on the way to get the required magnitude. This means that at $\theta_e=\theta_o$ the real part of the current vector becomes zero and hence subinterval #1 finishes when the line w intersects the current vector $\boldsymbol{I_1}$.

The angle θ_o is found by equating to zero the real part of (15) calculated at $\theta_e=\theta_o$ and is equal to

$$\theta_o = \frac{3\Omega_e LI}{V_d + 2E} \tag{24}$$

Substitution of $\theta_e=\theta_o$ in (15) results in only imaginary part and gives the current vector at the end of subinterval #1; it is

$$\boldsymbol{i_{1h}}(\theta_o)=-j\left[4\left(\frac{V_d-E}{V_d+2E}\right)\right]\frac{I}{\sqrt{3}} \tag{25}$$

As anticipated, the vector is aligned along $\boldsymbol{I_1}$ and has a magnitude lower than $2I/\sqrt{3}$.

During subinterval #2, the control system does not chop the VSI transistors T_6 and T_5 but keeps them ON to facilitate the incoming current to reach the required magnitude. Then only the legs b and c of the VSI conduct and the voltage of the neutral point of the motor with respect to o is $V_d/2$. Let us suppose that the leg a is fictitiously chopped at the voltage of $v_{ao} = e_a + V_d/2$ so as to maintain the zero current condition for the phase a. The other output voltages of the VSI are $v_{bo} = 0$ and $v_{co} = V_d$. Thus the vector of the output VSI voltages can be

determined and results in

$$V_{2h} = -\frac{2}{3}E - j\frac{1}{\sqrt{3}}V_d \tag{26}$$

whilst the vector of the voltage drops across the phase inductances becomes

$$V_{L,2h} = -j\frac{1}{\sqrt{3}}(V_d - 2E) \tag{27}$$

The two voltage vectors in (26) and (27) have both the magnitude and the slope that depend on the motor speed.

From (11) and (27), the current vector is given by

$$\boldsymbol{i_{2h}}(\theta_e - \theta_o) = -j\frac{1}{\sqrt{3}}\left(\frac{V_d - 2E}{\Omega_e L}\right)(\theta_e - \theta_o) + \boldsymbol{i_{1h}}(\theta_o) \tag{28}$$

Eqs. (25) and (28) points out that the tip of the current vector moves along the imaginary axis as shown in Fig. 8. Magnitude of the vector increases and then the tip continues to advance along $\boldsymbol{I_1}$ until it reaches the tip of $\boldsymbol{I_1}$ at $\theta_e = \theta_{ch}$. Duration of subinterval #2 is obtained by equating (28) at $\boldsymbol{I_1}$. It is

$$\theta_{co} \equiv \theta_{ch} - \theta_o = \frac{2\Omega_e LI(4E - V_d)}{(V_d - 2E)(V_d + 2E)} \tag{29}$$

and, from (24) and (29), the duration of the commutation interval is

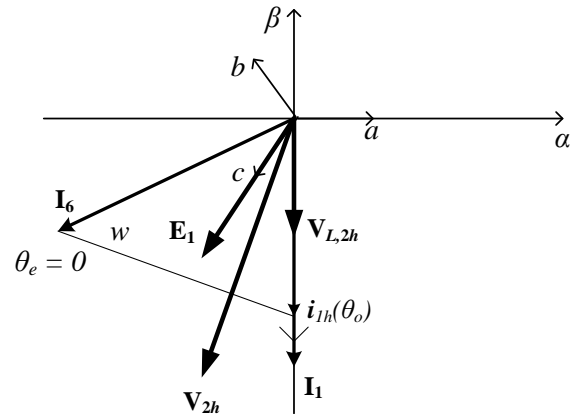$$\theta_{ch} = \frac{\Omega_e LI}{V_d - 2E} \tag{30}$$

Fig. 8. Phase vectors during subinterval #2 in high-speed zone.

The transients of the phase currents in the high-speed zone drawn in Fig. 5 (c) can be readily found by projecting the current vector on the axes a, b, and c of Fig. 8. As discussed in [9], in high-speed zone $\boldsymbol{i_{2h}}$ must equate $\boldsymbol{I_1}$ within $\theta_e=\pi/3$ to get

the required current reference at least at the end of the allowed commutation interval, i.e. of the supply interval.

IV. Effects of Current Commutations on Motor Torque

The instantaneous motor torque during current commutations can be still calculated by (5) and (9). For the current commutation occurring at the beginning of supply interval S_1, the instantaneous motor torque can be expressed as

$$\tau(\theta_e) = \frac{3}{2\Omega} E_1 \bullet i(\theta_e) \tag{31}$$

By (31), the torque changes during the commutation interval. The change is proportional to the projection of $[i(\theta_e) - I_1]$ on E_1 and, by accounting of the expressions of $i(\theta_e)$, the change is a linear function of θ_e.

In the low-speed zone, the projection of $i(\theta_e)$ on E_1 is greater than the projection of I_1 and the instantaneous motor torque has a positive dip. The torque ripple, which is the absolute of the maximum excursion, is equal to

$$TR_\ell = \left| \frac{3}{2} \left\{ \frac{E_1 \bullet [i_{1\ell}(\theta_i) - I_1]}{\Omega} \right\} \right| \tag{32}$$

After some manipulations the following expression is obtained for (32)

$$TR_\ell = \frac{n_p I}{\Omega_e} \left[\frac{(V_d - 4E)E}{V_d - E} \right] \tag{33}$$

In the high-speed zone, the projection of $i(\theta_e)$ on E_1 is lower than the projection of I_1 and the instantaneous motor torque has a negative dip. The torque ripple is now equal to

$$TR_h = \left| \frac{3}{2} \left\{ \frac{E_1 \bullet [i_{1h}(\theta_o) - I_1]}{\Omega} \right\} \right| \tag{34}$$

After some manipulations the following expression is obtained for (34)

$$TR_h = \left| \frac{2n_p I}{\Omega_e} \left[\frac{(4E - V_d)E}{V_d + 2E} \right] \right| \tag{35}$$

From Figs. 7 and 8, it can be easily realized that the torque ripple in both the low-speed and high-speed zones is proportional respectively to the maximum swing of the current of phase c.

Due to the torque dip, the motor torque, defined as the average value of the instantaneous motor torque over a supply period, changes with respect the expected value in (10), by increasing in the low-speed zone and decreasing in the high-speed zone. The terms in excess and in defect can be found by calculating the average value of the torque dip over the supply interval $\pi/3$. It comes out

$$\Delta T_\ell = \frac{3}{\pi} \frac{1}{2} TR_\ell \theta_{c\ell} \tag{36}$$

$$\Delta T_h = -\frac{3}{\pi} \frac{1}{2} TR_h \theta_{ch} \tag{37}$$

By substituting (23) and (33) into (36), and (30) and (35) into (37), the following expressions can be obtained for the two terms

$$\Delta T_\ell = \frac{3n_p L I^2}{4\pi} \left[\frac{V_d - 4E}{V_d - E} \right] \tag{38}$$

$$\Delta T_h = -\frac{3n_p L I^2}{\pi} \left[\frac{(4E - V_d)E}{(V_d + 2E)(V_d - 2E)} \right] \tag{39}$$

V. Exemplification

To demonstrate the potentialities of the vector approach in analyzing the operation of a PM BLDC drive, two control techniques of the VSI during the current commutations are considered, that have been proposed to eliminate the torque ripple produced by the commutations in the low-speed zone [13] and in the high-speed zone [14], respectively.

A. Low-speed zone

The control technique in [13] proposes to slow down reaching of the required magnitude from the incoming current i_b by forcing it to have a magnitude complementary to that one of the outgoing current i_a, i.e. by taking constant the sum of the magnitudes of i_b and i_a and equal to the required current magnitude $-I$. To fulfill this condition, [13] chops the transistor T_6 of the incoming phase during the commutation interval with the following duty-cycle:

$$\delta_\ell = \frac{4E}{V_d} \tag{40}$$

The VSI output voltages are then: $v_{ao} = V_d$, $v_{bo} = (1 - \delta_\ell)V_d$, $v_{co} = V_d$. By (7) and (11), the vectors of the VSI output voltages and the voltage drops across the phase inductance become

$$V_{1\ell} = \left[\frac{1}{3} - j \frac{1}{\sqrt{3}} \right] 4E \tag{41}$$

$$V_{L,1\ell} = \left[1 - j \frac{1}{\sqrt{3}} \right] 2E \tag{42}$$

Note that the voltage vector in (41) has the same direction as V_1 in (12) and a magnitude scaled of δ_ℓ. As it can be recognized from Fig. 9, this control technique forces the

voltage vector (42) to stay in parallel to the line joining I_6 and I_1 irrespectively from the motor speed, so that the current vector during the commutation moves along this line and its magnitude does not exhibit any positive swing. The commutation interval spans only subinterval #1 as the incoming current reaches the required magnitude at the same time as the outgoing current vanishes, and the commutation angle is still given by (23). Clearly, the duty-cycle in (40) can be applied only for $4E<V_d$, i.e. for $\delta_\ell <1$, and hence this technique is effective only in the low-speed zone.
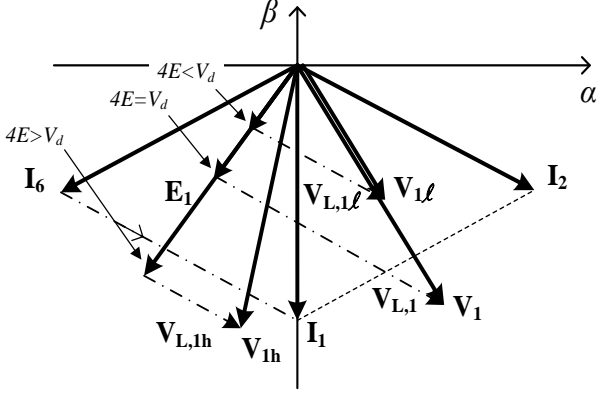

Fig. 9. PM BLDC control techniques to eliminate torque ripple.

B. High-speed zone

The control technique in [14] proposes to slow down vanishing of the outgoing current i_a by forcing it to have a magnitude complementary to that one of the incoming current i_b, i.e. by taking constant the sum of the magnitudes of i_b and i_a and equal to the required current magnitude -I. To fulfill this condition, [15] chops the transistor T_4 of the outgoing phase during the commutation interval with the following duty-cycle:

$$\delta_h = \frac{4E}{V_d} - 1 \tag{43}$$

The VSI output voltages are then: $v_{ao}=(1-\delta_h)V_d$, $v_{bo}=0$, $v_{co}=V_d$. By (7) and (11), the vectors of the VSI output voltages and the voltage drops across the phase inductance become

$$V_{1h} = \left(V_d - \frac{8}{3}E\right) - j\frac{1}{\sqrt{3}}V_d \tag{44}$$

$$V_{L,1h} = \left(1 - j\frac{1}{\sqrt{3}}\right)(V_d - 2E) \tag{45}$$

Note that direction of the vector in (44) depends on the motor speed; in spite of this, the vector in (45) is parallel to the line joining I_6 and I_1 irrespectively from the motor speed, as shown in Fig. 9, so that the current vector during the commutation moves along this line and does not exhibit any swing. Therefore this control technique operates in a similar way that

the technique in the low-speed zone but with the difference of chopping the output VSI voltage of the outgoing phase instead of the incoming one. As above, the commutation interval spans only subinterval #1 as the incoming current reaches the required magnitude at the same time as the outgoing current vanishes. Here, instead, the commutation angle changes with the speed and is given by

$$\theta_c = \frac{\Omega_e LI}{V_d - 2E} \tag{46}$$

As an example, Fig.10 gives the trajectory on the α,β plane of the current vector obtained without and with the control technique. The curves, obtained by simulation, clearly show the beneficial effect of the control.

The duty-cycle in (43) can be applied only for $4E>V_d$ and up to $2E=V_d$, i.e. for $\delta_h<1$, and hence this technique is effective only in the high-speed zone. Note that extension of (44)-(46) to the case of $2E=V_d$ leads to the situation where the DC link voltage is not more able to inject any current into the motor phases as the voltage drop on the phase inductances is zero.
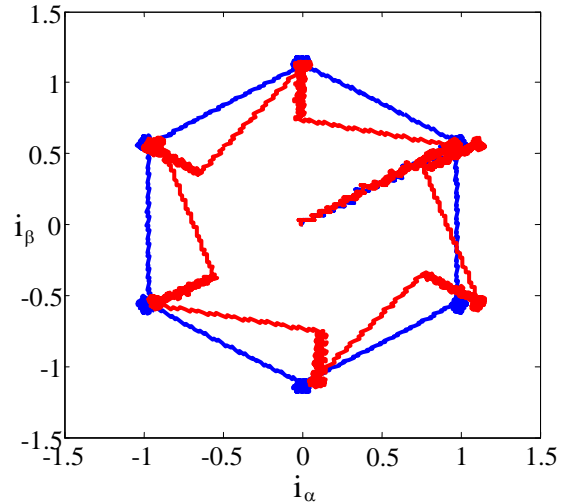

Fig. 10. Example of α,β plane trajectory of the current vector without (red line) and with (blue line) VSI control during the current commutations at high speed.

VI. CONCLUSIONS

The current transients during the commutations of the PM BLDC drives have been analyzed in the stationary plane with the help of the vector representation of the drive variables. Vectors of the VSI output voltages and the voltage drops on the phase inductances have been calculated and utilized to get the current vector trajectories for different motor speeds as well as to find out the commutation intervals. The results of the analysis have been used to obtain the motor torque and the torque ripples due to the current commutations. Lastly, the vector approach has been applied to two control techniques of the PM BLDC drives with the end of explaining how they operate to eliminate the torque ripples due to the current commutations.

REFERENCES

[1] P.Pillay and R.Krishnan, "Application characteristics of permanent magnet synchronous and brushless DC motors for servo drives," *IEEE Trans. on Industry Applications*, vol.27, no.5, pp.986-996, Sept./Oct. 1991.

[2] T. S. Low, T. H. Lee, K. J. Tseng, and K. S. Lock, "Servo performance of a BLDC drive with instantaneous torque control," *IEEE Trans. on Industry Applications*, vol. 28, no. 2, pp. 455- 462, Mar./Apr. 1992.

[3] A.Sathyan, M.Krishnamurthy, N.Milivojevic, and A.Emadi, "A low-cost digital control scheme for Brushless DC motor drives in domestic applications", in Proc. of IEEE Electric Machines and Drives Conf. (IEMDC), 2009, pp. 76-82.

[4] K.T.Chau, C.C.Chan, and C.Liu, "Overview of permanent-magnet brushless drives for electric and hybrid electric vehicles," *IEEE Trans. on Industrial Electronics*, vol. 55, no. 6, pp. 2246-2257, Jun. 2008.

[5] G.Buja and M.Bertoluzzo, "Development of electric propulsion systems for light electric vehicles," *IEEE Trans. on Industrial Informatics*, vol.7, no.3, pp.428-435, Aug. 2011.

[6] A.M.El-Refaie, "Motors/generators for traction/propulsion applications: a review," *IEEE Vehicular Technology Magazine*, vol. 8, no. 1, pp. 90-99, March 2013.

[7] T.Kenjo and S.Nagamore, "Permanent-Magnet and Brushless DC Motors", Oxford, U.K.: Clarendon, 1985.

[8] R.Krishnan, "Permanent magnet synchronous motors and brushless DC motor drives", Taylor & Francis, CRC Press, Boca Raton, 2010.

[9] T.J.E.Miller, "Brushless permanent-magnet and reluctance motor drives", Oxford, U.K.: Clarendon, 1989.

[10] P.Pillay and K.Ramu, "Modeling, simulation and analysis of permanent magnet motor drives, Part II: the brushless DC motor drive", *IEEE Trans. on Industry Applications*, vol. 25, no. 2, pp. 274-279, March April 1989.

[11] R.Carlson, M.Lajoie-Mazenc, and J.C. dos S.Fagundes, "Analysis of torque ripple due to phase commutation in brushless DC machine," *IEEE Trans. on Industry Applications*, vol.28, no.3, pp.632-638, May/Jun. 1992.

[12] G.Buja, M.Bertoluzzo, R.Keshri, and R.Menis, "Stationary plane based investigation of the behavior of PM BLDC Drives", in Proc. of IEEE Annual Conf. on Industrial Electronics (IECON), 2013, pp. 6630-6635.

[13] J.Fang, H.Li, and B.Han, "Torque ripple reduction in BLDC torque motor with nonideal back EMF", *IEEE Trans. on Power Electronics*, vol.27, no.11, pp. 4630-4637, Nov. 2012

[14] J.H.Song and I.Choy, "Commutation torque ripple reduction in brushless DC motor drives using a single DC current sensor", *IEEE Trans. on Power Electronics*, vol.19, no.2, pp. 312-319, March 2004.